MAGNETOHYDRODYNAMICS Vol. 57 (2021), No. 3, pp. 385–404
DOI: 10.22364/mhd.57.3.7

MAGNETOHYDRODYNAMIC FLOW OF HYBRID Ag-CuO/H_2O NANOFLUID PAST A STRETCHING/SHRINKING POROUS PLATE WITH VISCOUS-OHMIC DISSIPATION AND HEAT GENERATION/ABSORPTION

Rusya Iryanti Yahaya [1,*], *Norihan Md Arifin* [2]

[1] *Institute for Mathematical Research, University Putra Malaysia, 43400 UPM Serdang, Selangor Darul Ehsan, Malaysia*
[2] *Department of Mathematics, University Putra Malaysia, 43400 UPM Serdang, Selangor Darul Ehsan, Malaysia*
[*] *Corresponding author's e-Mail: rusyairyanti@gmail.com*

The idea of hybridising different nanoparticles arises from the attempt to find efficient working fluids with better hydrodynamic and thermophysical properties for heat transfer applications. Rapid studies are carried out to understand the flow and thermal behaviours of the hybrid nanofluid in different flow geometries and conditions. In this paper, a flow of Ag-CuO/H_2O hybrid nanofluid past a porous stretching/shrinking plate in the presence of suction, magnetic field, viscous-Ohmic dissipation, and heat generation/absorption is studied. Governing equations and boundary conditions are transformed into a system of ordinary differential equations using similarity transformations and are computed numerically using the `bvp4c` solver. The numerical solutions presented in tables and graphs are analysed. The velocity profile for the stretching plate diminishes with the increment of the dimensionless parameters of the magnetic field, suction, local porosity, and nanoparticle volume fraction of Ag, but an opposite situation occurred for the shrinking plate. However, the increase of the heat generation parameter and Eckert number decreases the Nusselt number. The high heat transfer performance of the Ag-CuO/H_2O hybrid nanofluid is disturbed by the presence of heat generation and viscous-Ohmic dissipation in the flow.

Introduction.

A new generation of nanofluids termed the hybrid nanofluid comprises two or more different nanoparticles dispersed in a base fluid. Metallic nanoparticles (e.g., Cu, Al, and Ag) have a high thermal conductivity but are chemically reactive and unstable, whereas oxide nanoparticles (e.g., Al_2O_3, CuO, and ZnO) are chemically inert and stable but have a low thermal conductivity [1]. Dispersing these different types of nanoparticles in a base fluid (e.g., water (H_2O), ethylene glycol (EG), and kerosene) can provide better thermophysical and hydrodynamic properties than conventional nanofluids and base fluids. Researchers are rapidly studying the synthesis and preparation of different hybrid nanofluids to find the optimum combination of nanoparticles and base fluid. In the field of fluid dynamics, the thermal and rheological behaviour of different hybrid nanofluids, such as Cu-Al_2O_3/H_2O, Ag-CuO/H_2O, and Cu-TiO_2/EG, under different flow conditions are analyzed for diverse potential applications, for instance, in technology, engineering, and in medicine. For example, Chahregh and Dinarvand [2] studied a flow of $Ti0_2$-Ag/blood hybrid nanofluid through a porous channel by modelling the drug delivery in the arterial blood flow for medical and treatment applications. Rajesh *et al.* [3] analyzed the heat transfer and flows of CuO/H_2O nanofluid and Ag-CuO/H_2O hybrid nanofluid over a moving oscillating cylinder. The hybrid nanofluid exhibits a superior heat transfer

performance and a lower skin friction coefficient than the nanofluid. Fluid flows over stretching/shrinking surfaces occurr in different industrial processes, such as the production of paper, wire drawing, and extraction of plastic sheets and plastic films [4]. The stagnation point flow of hybrid Ag-CuO/H_2O nanofluid over a stretching/shrinking sheet with suction/injection was discussed by Arani and Aberoumand [5]. The increase in suction/injection parameter was found to enhance the physical quantities of interest, i.e. the Nusselt number and the skin friction coefficient of the hybrid nanofluid.

Magnetohydrodynamics (MHD), a reserach branch in fluid dynamics, deals with the behaviour of conducting fluids in the presence of a magnetic field. The importance of the MHD boundary layer flow of fluid is considered in petroleum industries, geothermal engineering, nuclear reactors, and aerodynamics [6]. Devi and Devi [7] studied an magnetohydrodynamic flow of an aqueous hybrid Cu-Al_2O_3 nanofluid past a permeable stretching sheet with suction and found that the flow becomes consistent and the rate of heat transfer increases due to the magnetic field. Nadeem and Abbas [8] revealed that the Lorentz force produced by the interaction of the magnetic field and the moving micropolar hybrid nanofluid stabilizes the viscous impacts in the fluid and boosts the fluid velocity. However, this force decreases the velocity of the Cu-Al_2O_3/H_2O hybrid nanofluid flow over a stretching/shrinking flat plate with suction/injection [9]. The same result was obtained by Waini *et al.* [10], where the magnetic field promotes the increase of the Nusselt number and skin friction coefficient. Yashkun *et al.* [11] discussed the MHD Cu-Al_2O_3/H_2O hybrid nanofluid flow past a stretching/shrinking sheet with suction and thermal radiation. Increasing the suction and thermal radiation parameters increases the skin friction coefficient, whereas the Nusselt number increases with suction but decreases with the thermal radiation parameter. Other studies on MHD flow have been done by Jimenez *et al.* [12], Klüber *et al.* [13] and Mao *et al.* [14].

Temperature variations of the surrounding fluid and surface by heat generation or absorption may occur in practical industrial and engineering applications, for example, in nuclear reactors, electronic chips, and semiconductor wafers. Therefore, it is worth investigating the effects of the heat generation/absorption parameter on the temperature field, especially, for problems involving chemical reactions and dissociating fluids, as it may change the particle deposition rate and the heat transfer capability [15–17]. Hayat and Nadeem [18] studied the effects of heat generation on the rotating flow of Ag-CuO/H_2O hybrid nanofluid past a stretching surface and found that the heat generation parameter enhances the temperature field due to the production of energy at the thermal boundary layer of the fluid. Later, Hayat *et al.* [19] extended this study with additional magnetic field parameters. It was observed that the temperature profile increases with the increasing values of magnetic, rotation and heat generation/absorption parameters. Meanwhile, Zainal *et al.* [20] reported that the heat transfer performance decreases due to the presence of heat generation, but it improves with the appearance of heat absorption in the MHD flow of the Al_2O_3-Cu/H_2O hybrid nanofluid.

Other physical parameters that attract attention of researchers are viscous and Ohmic dissipations. Viscous dissipation is an irreversible process in which the kinetic energy is transformed into heat by the work against viscous stresses [17]. Whereas, Ohmic dissipation describes the conversion of electrical energy into heat when a current passes through a resistance [21]. The viscous and Ohmic dissipations play a significant role in increasing the surface temperature in some industrial processes, for example, in polymer processing flows and aerodynamics heating [17, 22]. Jusoh *et al.* [23] observed that the increase of the viscous dissipation parameter increases the fluid temperature but

decreases the Nusselt number in the Ag-Cu/H_2O hybrid nanofluid flow past a stretching/shrinking surface. The increase in fluid temperature caused by viscous dissipation was also reported by Lund *et al.* [24] in the Cu-Al_2O-3/H_2O hybrid nanofluid flow past a shrinking surface. Similar behaviours were observed in the studies of Ohmic dissipation effects on MHD flow of hybrid nanofluids. Khashiie *et al.* [25] found that the presence of Ohmic dissipation in the flow does not produce any significant effect on the skin friction coefficient but decreases the Nusselt number that corresponds to the heat transfer rate. Besides, the temperature profile of the hybrid nanofluid increases with the increase of the Ohmic dissipation parameter. The same results were obtained in the studies by Yashkun *et al.* [26], Yan *et al.* [27] and Mahanthesh *et al.* [28].

Fluid flow past a stretching/shrinking surface arises in different industrial applications, such as extrusion of plastic sheets, glass blowing, and hot rolling. Inspired by the previous studies, the MHD flow of Ag-CuO/H_2O hybrid nanofluid past a stretching/shrinking plate with suction and heat generation/absorption is studied. Since MHD flow is considered in the current study, it is interesting to analyze the viscous-Ohmic dissipation effects on the flow. The governing equations and boundary conditions will be reduced to a system of ordinary differential equations using similarity transformations. Numerical solutions will be then computed using a MATLAB solver `bvp4c` and will be tabulated and presented graphically. The impact of several parameters on the hybrid nanofluid flow and physical quantities of interest, which are the Nusselt number and the skin friction coefficient, will also be analyzed and discussed. The findings of this study are expected to provide some insight for the interested parties, especially the engineering communities, for potential real-life applications or future research.

1. Mathematical formulation.

Effects of different physical parameters on the incompressible, laminar, two-dimensional flow of Ag-CuO/H_2O hybrid nanofluid over a vertical flat plate are studied. The Cartesian coordinates x and y are designated to be the regions that are parallel and perpendicular to the flat plate, respectively. The plate has a non-linear velocity $u_w(x) = ax^m$, with a and m being the constants related to the stretching/shrinking velocity. Whereas, the mass transfer velocity along the y-axis is given by v_w and the alternating magnetic field is $B(x) = B_0 x^{(m-1)/2}$ with B_0 as a constant for the magnetic field strength. The induced magnetic field is excluded from this study due to the assumption of an extremely small magnetic Reynolds number. The working fluid, hybrid Ag-CuO/H_2O nanofluid, comprises Ag and CuO nanoparticles, with water as the base fluid, and the thermophysical properties are given in Table 1. Hereafter, the subscripts 'hnf', 'nf', 'f', 'bf', 's1' and 's2' represent hybrid nanofluid, nanofluid, base fluid, solid, CuO nanoparticles, and Ag nanoparticles, respectively. The base fluid and the nanoparticles are assumed to be in thermal equilibrium. A schematic diagram of the studied problem is illustrated in Fig. 1.

Table 1. Thermophysical properties [29].

Physical properties	H_2O, f	CuO, $s1$	Ag, $s2$
Density ϱ, [kg/m^3]	997.1	6320	10 500
Specific heat capacity C_p, [J/ kg K]	4179	531.8	235
Thermal conductivity k, [W/ m K]	0.613	76.5	429
Electrical conductivity σ, [S/m]	0.05	$2.7{\cdot}10^{-8}$	$6.3{\cdot}10^{7}$

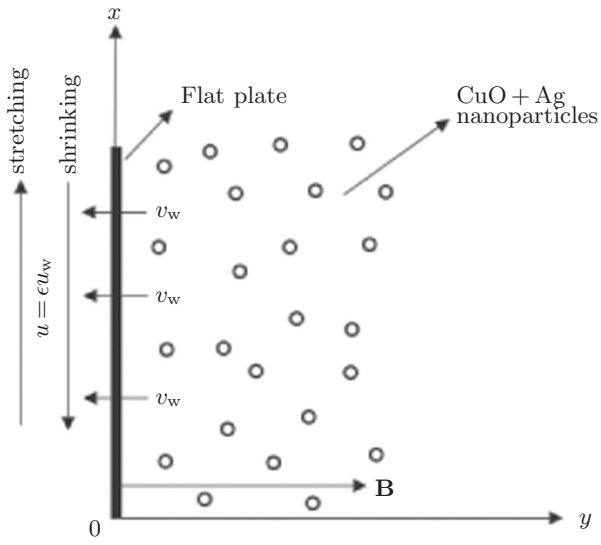

Fig. 1. Schematic presentation of the problem and coordinate system.

The governing equations and the boundary conditions for the considered problem are the following.

The continuity equation:

$$\frac{\partial u}{\partial x} + \frac{\partial v}{\partial y} = 0. \tag{1}$$

The momentum equation:

$$u\frac{\partial u}{\partial x} + v\frac{\partial u}{\partial y} = \frac{1}{\varrho_{\mathrm{hnf}}}\left(\mu_{\mathrm{hnf}}\frac{\partial^2 u}{\partial y^2} - \sigma_{\mathrm{hnf}}B(x)^2 u\right) - \frac{\mu_{\mathrm{hnf}}}{K}u. \tag{2}$$

The energy equation:

$$\begin{aligned} u\frac{\partial T}{\partial x} + v\frac{\partial T}{\partial y} = {} & \frac{k_{\mathrm{hnf}}}{(\varrho C_{\mathrm{p}})_{\mathrm{hnf}}}\frac{\partial^2 T}{\partial y^2} + \frac{\mu_{\mathrm{hnf}}}{(\varrho C_{\mathrm{p}})_{\mathrm{hnf}}}\left(\frac{\partial u}{\partial y}\right)^2 \\ & + \frac{\sigma_{\mathrm{hnf}}B(x)^2u^2}{(\varrho C_{\mathrm{p}})_{\mathrm{hnf}}} + \frac{Q_0}{(\varrho C_{\mathrm{p}})_{\mathrm{hnf}}}(T - T_\infty). \end{aligned} \tag{3}$$

The boundary conditions:

$$u = \epsilon u_{\mathrm{w}}, \quad v = v_{\mathrm{w}}, \quad T = T_{\mathrm{w}} \quad \text{at } y = 0, \tag{4}$$

$$u \to 0, \quad T \to T_\infty \quad \text{as } y \to \infty, \tag{5}$$

where u is the velocity component in the x-direction, v is the velocity component in the y-direction, K is the permeability of the porous medium, Q_0 is the heat generation/absorption coefficient and T is the fluid temperature with the subscripts 'w' and '∞' to denote the fluid temperature at the surface and at the free flow, respectively. Meanwhile, the relationship between the physical quantities of the hybrid nanofluid, base fluid and nanoparticles is given in Table 2.

Table 2. Physical quantities of nanofluid and hybrid nanofluid [7].

Properties	Hybrid Nanofluid
ϱ	$\varrho_{\rm hnf}=(1-\phi_{\rm s2})[(1-\phi_{\rm s1})\varrho_{\rm f}+\phi_{\rm s1}\varrho_{\rm s1}]+\phi_{\rm s2}\varrho_{\rm s2}$
$\varrho C_{\rm p}$	$(\varrho C_{\rm p})_{\rm hnf}=(1-\phi_{\rm s2})[(1-\phi_{\rm s1})(\varrho C_{\rm p})_{\rm f}+\phi_{\rm s1}(\varrho C_{\rm p})_{\rm s1}]+\phi_{\rm s2}(\varrho C_{\rm p})_{\rm s2}$
μ	$\mu_{\rm hnf}=\dfrac{\mu_{\rm f}}{(1-\phi_{\rm s1})^{2.5}(1-\phi_{\rm s2})^{2.5}}$
k	$\dfrac{k_{\rm hnf}}{k_{bf}}=\dfrac{k_{\rm s2}+2k_{bf}-2\phi_{\rm s2}(k_{bf}-k_{\rm s2})}{k_{\rm s2}+2k_{bf}+\phi_{\rm s2}(k_{bf}-k_{\rm s2})}$ where $\dfrac{k_{bf}}{k_{\rm f}}=\dfrac{k_{\rm s1}+2k_{\rm f}-2\phi_{\rm s1}(k_{\rm f}-k_{\rm s1})}{k_{\rm s1}+2k_{\rm f}+\phi_{\rm s1}(k_{\rm f}-k_{\rm s1})}$
σ	$\dfrac{\sigma_{\rm hnf}}{\sigma_{bf}}=\dfrac{\sigma_{\rm s2}+2\sigma_{bf}-2\phi_2(\sigma_{bf}-\sigma_{\rm s2})}{\sigma_{\rm s2}+2\sigma_{bf}+\phi_2(\sigma_{bf}-\sigma_{\rm s2})}$ where $\dfrac{\sigma_{bf}}{\sigma_{\rm f}}=\dfrac{\sigma_{\rm s1}+2\sigma_{\rm f}-2\phi_1(\sigma_{\rm f}-\sigma_{\rm s1})}{\sigma_{\rm s1}+2\sigma_{\rm f}+\phi_1(\sigma_{\rm f}-\sigma_{\rm s1})}$

The following similarity transformations are applied to Eqs. (1)–(5),

$$\begin{aligned}
&\psi=\sqrt{\frac{2\nu_{\rm f}u_{\rm w}x}{(m+1)}}f(\eta),\quad \eta=\sqrt{\frac{(m+1)u_{\rm w}}{2\nu_{\rm f}x}}y,\\
&u=ax^m f'(\eta),\quad v=-\sqrt{\frac{1}{2}(m+1)\nu_{\rm f}ax^{m-1}}\left[f(\eta)+\left(\frac{m-1}{m+1}\right)\eta f'(\eta)\right],\\
&\theta(\eta)=\frac{T-T_\infty}{T_{\rm w}-T_\infty},
\end{aligned}\tag{6}$$

with η being the similarity variable, $\theta(\eta)$ the dimensionless temperature and ψ the stream function, to derive the following non-linear ordinary differential equations and boundary conditions:

$$\begin{aligned}
&f'''-(1-\phi_{\rm s1})^{2.5}(1-\phi_{\rm s2})^{2.5}\left[(1-\phi_{\rm s2})\left[(1-\phi_{\rm s1})+\phi_{\rm s1}\frac{\varrho_{\rm s1}}{\varrho_{\rm f}}\right]+\phi_{\rm s2}\frac{\varrho_{\rm s2}}{\varrho_{\rm f}}\right]\\
&\times\left(\frac{2m}{m+1}f'^2-ff''\right)-\frac{2}{m+1}\Bigg((1-\phi_{\rm s1})^{2.5}(1-\phi_{\rm s2})^{2.5}\frac{\sigma_{\rm hnf}}{\sigma_{\rm f}}{\rm M}\\
&+\left[(1-\phi_{\rm s2})\left[(1-\phi_{\rm s1})+\phi_{\rm s1}\frac{\varrho_{\rm s1}}{\varrho_{\rm f}}\right]+\phi_{\rm s2}\frac{\varrho_{\rm s2}}{\varrho_{\rm f}}\right]\lambda\Bigg)f'=0,
\end{aligned}\tag{7}$$

$$\begin{aligned}
&\theta''+\left[(1-\phi_{\rm s2})\left[(1-\phi_{\rm s1})+\phi_{\rm s1}\frac{(\varrho C_{\rm p})_{\rm s1}}{(\varrho C_{\rm p})_{\rm f}}\right]+\phi_{\rm s2}\frac{(\varrho C_{\rm p})_{\rm s2}}{(\varrho C_{\rm p})_{\rm f}}\right]\frac{k_{\rm f}}{k_{\rm hnf}}\,{\rm Pr}\,f\theta'\\
&+\frac{2}{m+1}\frac{k_{\rm f}}{k_{\rm hnf}}\,{\rm Pr}\left[\frac{\sigma_{\rm hnf}}{\sigma_{\rm f}}{\rm MEc}f'^2+{\rm Q}\theta\right]+\frac{k_{\rm f}}{k_{\rm hnf}}\frac{{\rm Pr\,Ec}}{(1-\phi_{\rm s1})^{2.5}(1-\phi_{\rm s2})^{2.5}}f''^2=0,
\end{aligned}\tag{8}$$

$$\begin{aligned}
&f(0)=S,\quad f'(0)=\epsilon,\quad \theta(0)=1,\\
&f'(\infty)\to 0,\quad \theta(\infty)\to 0.
\end{aligned}\tag{9}$$

Prime (') indicates the derivative with respect to η, whereas ϵ is the stretching/shrinking parameter, with $\epsilon>0$ for stretching and $\epsilon<0$ for shrinking, $\phi_{\rm s1}$ is the nanoparticle volume fraction of CuO and $\phi_{\rm s2}$ is the nanoparticle volume fraction of Ag. The magnetic parameter M, the local porosity parameter λ, the Prandtl number Pr, the Eckert number Ec, the suction parameter S(>0), and the heat generation/absorption parameter Q, with

$\mathrm{Q} > 0$ for heat generation and $\mathrm{Q} < 0$ for heat absorption, are given as follows:

$$\mathrm{M} = \frac{\sigma_\mathrm{f} B_0^2}{\varrho_\mathrm{f} a}, \quad \lambda = \frac{\mu_\mathrm{f}}{K a x^{m-1}}, \quad \mathrm{Pr} = \frac{\nu_\mathrm{f} (\varrho C_\mathrm{p})_\mathrm{f}}{k_\mathrm{f}},$$

$$\mathrm{Ec} = \frac{u_\mathrm{w}^2}{(C_\mathrm{p})_\mathrm{f}(T_\mathrm{w} - T_\infty)}, \quad \mathrm{Q} = \frac{\mathrm{Q}_0 x}{(\varrho C_\mathrm{p})_\mathrm{f} u_\mathrm{w}}, \quad \mathrm{S} = -v_\mathrm{w} \sqrt{\frac{2}{(m+1)\nu_\mathrm{f} a x^{m-1}}},$$

with ν_f being the kinematic viscosity of the base fluid.

The skin friction coefficient C_f and the Nusselt number Nu are defined as

$$C_\mathrm{f} = \frac{2\mu_\mathrm{hnf}}{\varrho_\mathrm{f} u_\mathrm{w}^2} \left(\frac{\partial u}{\partial y}\right)_{y=0}, \quad \mathrm{Nu} = -\frac{k_\mathrm{hnf} x}{k_\mathrm{f}(T_\mathrm{w} - T_\infty)} \left(\frac{\partial T}{\partial y}\right)_{y=0},$$

which are reduced to the following dimensionless form of the skin friction coefficient and Nusselt number

$$C_\mathrm{f} \mathrm{Re}_x^{1/2} = \frac{\sqrt{2(m+1)}}{(1-\phi_{\mathrm{s}1})^{2.5}(1-\phi_{\mathrm{s}2})^{2.5}} f''(0), \quad \mathrm{Nu}\mathrm{Re}_x^{-1/2} = -\frac{k_\mathrm{hnf}}{k_f} \sqrt{\frac{m+1}{2}} \theta'(0), \tag{10}$$

where $\mathrm{Re}_x = x u_\mathrm{w}/\nu_\mathrm{f}$ is the local Reynolds number.

2. Numerical solution.

The numerical solution of the non-linear ordinary differential equations (7) and (8) and the boundary conditions (9) is computed using the MATLAB built-in residual control based adaptive mesh solver `bvp4c`. This solver is a finite difference code that implements the three-stage Lobatto IIIa formula, and the effectiveness depends on the algorithm with an initial guess for the solution. An initial guess for the desired solution for the boundary value problems (BVPs) is required when working with the BVP codes, and this is a challenge to the user. However, the `bvp4c` solver has an unusual approach to control errors that helps to deal with poor guesses to give an accurate numerical solution [30].

The calling function of `bvp4c` is `sol=bvp4c(odefun, bcfun, solinit)`. The first step of using the `bvp4c` solver is to rewrite Eqs. (7)–(9) as a system of first-order ordinary differential equations by introducing new variables for each derivative up to one less than the highest derivatives appearing in the equations. A detailed explanation of this process is presented by Ferdows *et al.* [31]. The modified differential equations are then coded into `odefun`, the boundary conditions are coded into `bcfun` and the initial guess is made in `solinit`.

The numerical scheme used in this study is validated by comparing with previously published studies. As presented in Table 3, the obtained numerical results are compared with the previous results by Upreti *et al.* [32] and Elbashbeshy *et al.* [33]. The results

Table 3. Values of $-\theta'(0)$ when $m = 1$, $\epsilon = 1$ and $\phi_{\mathrm{s}1} = \phi_{\mathrm{s}2} = \mathrm{Ec} = \mathrm{M} = \mathrm{S} = \mathrm{Q} = \lambda = 0$.

	$-\theta'(0)$		
Pr	Present	[32]	[33]
1.0	0.581976711	0.5818299	0.5820
10.0	2.308003948	2.3079730	2.3080

reported by in [32] and in [33] were computed using the shooting method and a function in Mathematica, respectively, thus, providing a good comparison for the results obtained by different numerical schemes. Since the results are in good agreement, the accuracy of the method used in the present study is validated.

3. Results and discussion.

Different parameters, such as the magnetic parameter M, the Eckert number Ec, the local porosity parameter λ, the heat generation/absorption parameter Q, the stretching/shrinking parameter ϵ, the suction parameter S and the Prandtl number Pr are included in the governing equations and boundary conditions for the hybrid Ag-CuO/H_2O nanofluid flow past a flat plate. The values of these parameters are varied during computation, and the resulting numerical solutions are presented in tables and graphs for further analysis and discussion. The accuracy of the numerical solutions is verified as the velocity and temperature profiles reach the free flow boundary conditions (9), asymptotically.

The variation of the physical quantities of interest, $C_f \mathrm{Re}_x^{1/2}$ and $\mathrm{Nu}\mathrm{Re}_x^{-1/2}$ with

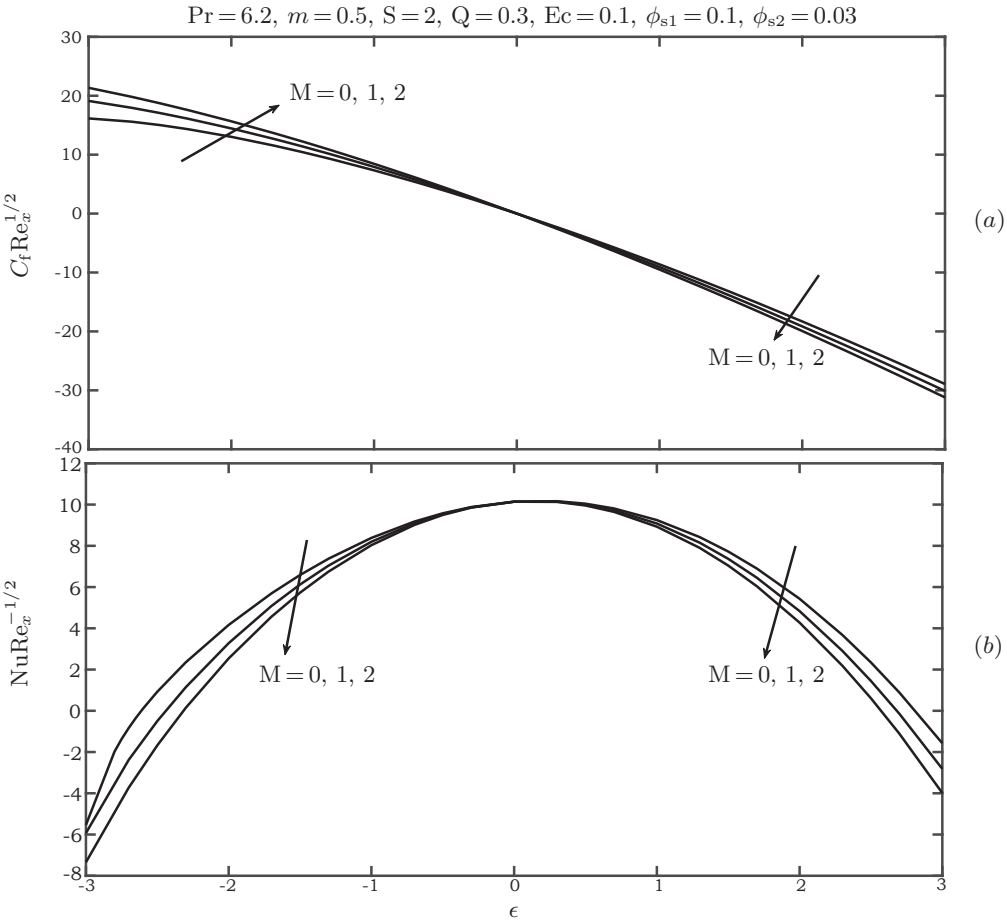

Fig. 2. Variation of (*a*) skin friction coefficient $C_f \mathrm{Re}_x^{1/2}$ and (*b*) Nusselt number $\mathrm{Nu}\mathrm{Re}_x^{-1/2}$ with different values of M.

multiple values of M is illustrated in Figs. 2. As shown in Fig. 2*a*, the increase in the magnetic parameter M enhances the skin friction coefficient for $\epsilon < 0$ (shrinking plate case), but the opposite behaviour is observed for $\epsilon > 0$ (stretching plate case). The values of $C_{\mathrm{f}}\mathrm{Re}_x^{1/2}$ are noted to be positive for the shrinking plate, whereas they are negative for the stretching plate. Arifin *et al.* [34] stated that the positive value of the skin friction coefficient implies that the fluid exerted a drag force to the surface, and the negative value indicates the opposite. Meanwhile, it is observed from Fig. 2*b* that the Nusselt number, which corresponds to the heat transfer rate at the surface, is the highest in the absence of the magnetic field ($\mathrm{M} = 0$) and decreases as M increases in both cases of the shrinking and the stretching plate. Regardless of the value of the other parameters, the skin friction coefficient is zero when $\epsilon = 0$ because there is no shear stress at the surface when the plate and the fluid are static, yet, the transfer of heat between the plate and the fluid still happens due to the temperature difference between the two media. Contrary to the stretching plate, the velocity profile $f'(\eta)$ of the hybrid nanofluid for the shrinking plate case increases with M. The imposition of a magnetic field on the hybrid nanofluid flow produces a Lorentz force that impedes the flow and causes the momentum boundary layer thickness to reduce, as shown in Fig. 3. The velocity gradient at the surface ($f''(0)$) then increases for the shrinking plate and decreases for the stretching plate, which is consistent with the results obtained for

$$C_{\mathrm{f}}\mathrm{Re}_x^{1/2}\left(=\frac{\sqrt{2(m+1)}}{(1-\phi_{\mathrm{s}1})^{2.5}(1-\phi_{\mathrm{s}2})^{2.5}}f''(0)\right).$$

However, the Lorentz force increases the temperature of the hybrid nanofluid and increases the thermal boundary layer thickness. Since the Lorentz force is a retarding force that resists the fluid flow, the hybrid nanofluid has to do extra work that later can be converted into thermal energy and increases the fluid temperature [35]. This impact is more pronounced in the shrinking plate case, as shown in Fig. 4.

The effect of the suction parameter S on $C_{\mathrm{f}}\mathrm{Re}_x^{1/2}$ and $\mathrm{Nu}\mathrm{Re}_x^{-1/2}$ is illustrated in Figs. 5*a* and 5*b*, respectively. A different behaviour is observed for the shrinking and stretching plate cases when the value of $C_{\mathrm{f}}\mathrm{Re}_x^{1/2}$ increases for $\epsilon < 0$ but decreases for $\epsilon > 0$ when S increases, as shown in Fig. 5*a*. The imposition of suction reduces the

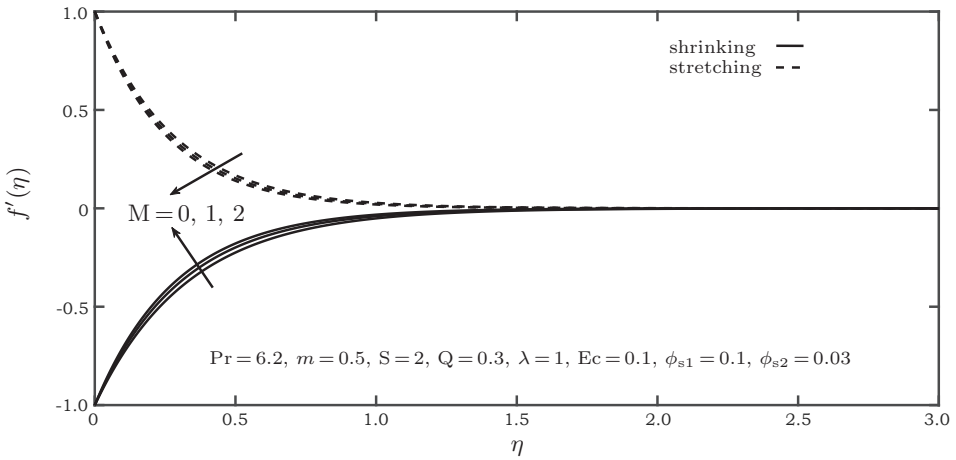

Fig. 3. Velocity profiles, $f'(\eta)$ with different values of M.

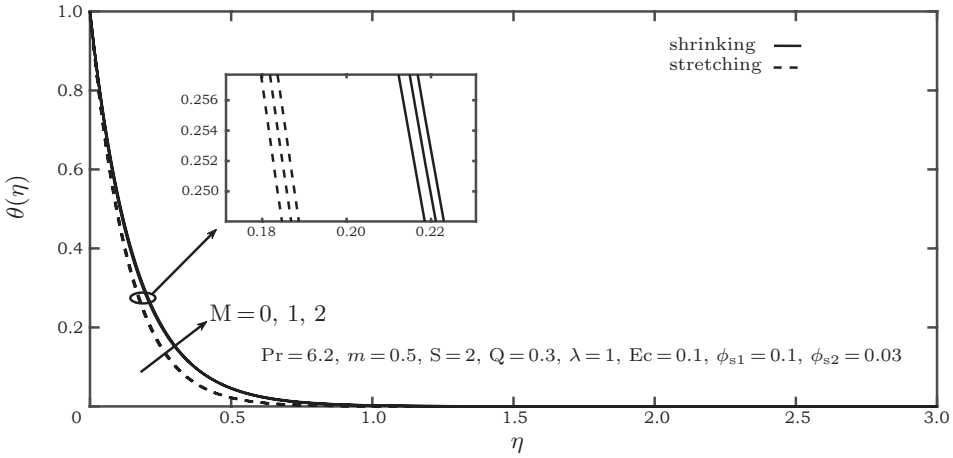

Fig. 4. Temperature profiles, $\theta(\eta)$ with different values of M.

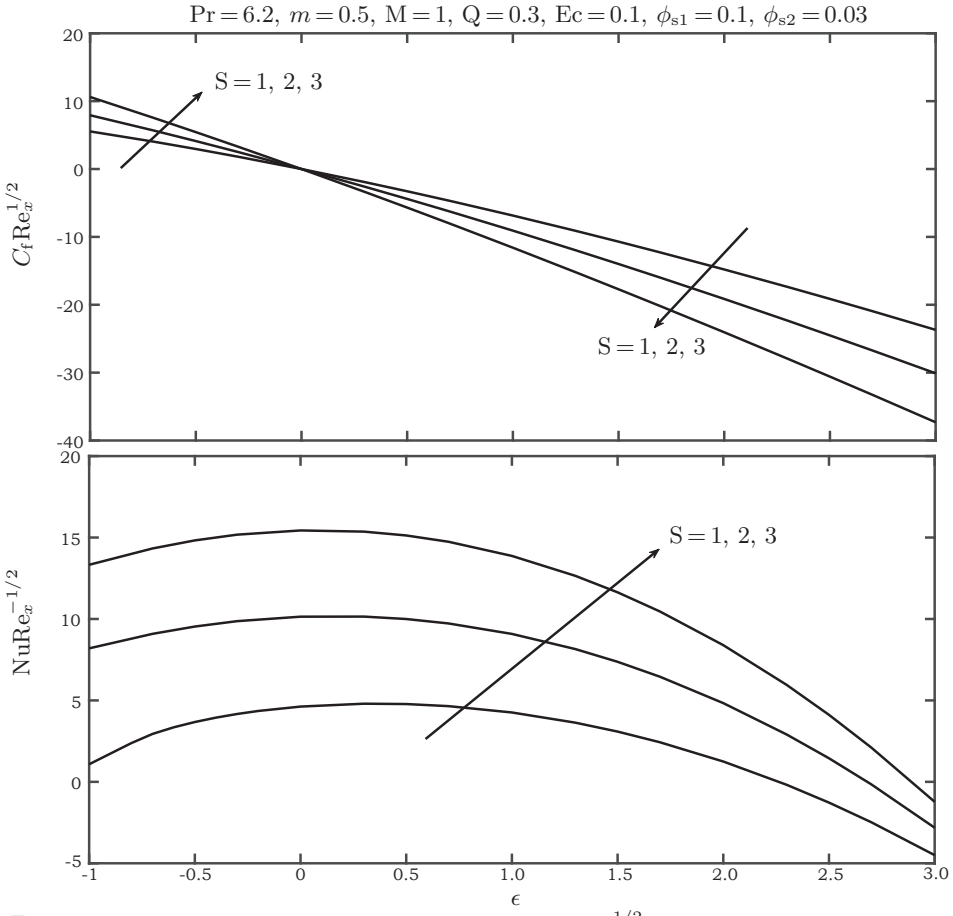

Fig. 5. Variation of (*a*) skin friction coefficient $C_f \mathrm{Re}_x^{1/2}$ and (*b*) Nusselt number $\mathrm{NuRe}_x^{-1/2}$ with different values of S.

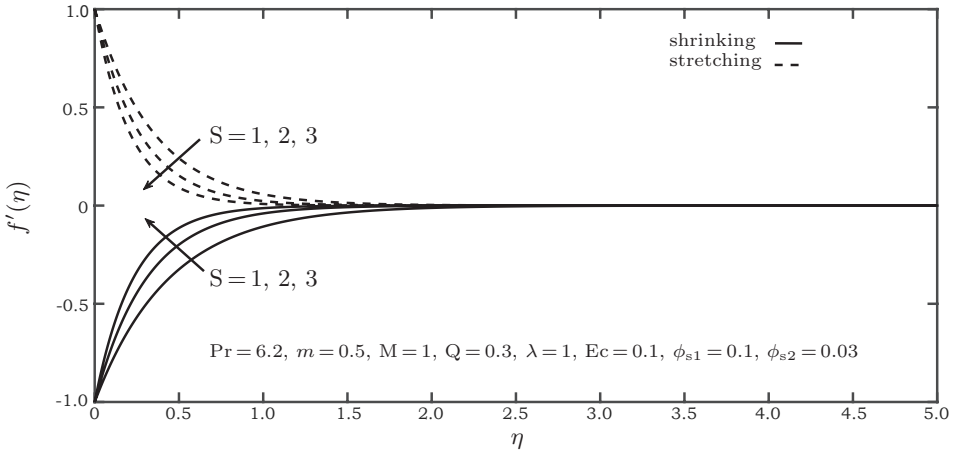

Fig. 6. Velocity profiles, $f'(\eta)$ with different values of S.

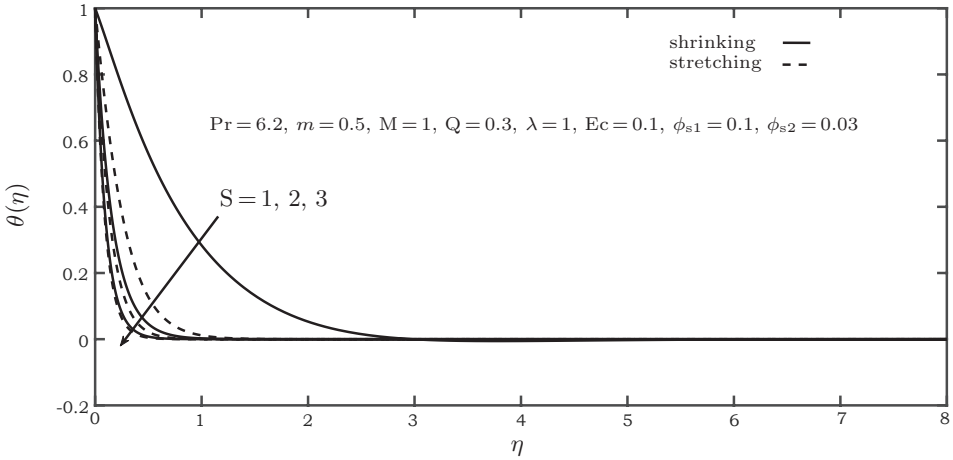

Fig. 7. Temperature profiles, $\theta(\eta)$ with different values of S.

momentum boundary layer thickness, which increases and decreases the velocity gradient at the surface of the shrinking and the stretching plate, respectively. Then, the velocity profile increases for the shrinking plate but decreases for the stretching plate, as shown in Fig. 6. Besides, the increase in suction causes the thermal boundary layer thickness to reduce and increases the temperature gradient at the surface ($\theta'(0)$) which then increases the Nusselt number, as shown in Fig. 5*b*. As suction is imposed on the plate surface, a warmer fluid is taken away from the boundary layer and causes the temperature profile to drop, as illustrated in Fig. 7.

Next, the variations of $C_{\mathrm{f}}\mathrm{Re}_x^{1/2}$, $\mathrm{NuRe}_x^{-1/2}$, $f'(\eta)$ and $\theta(\eta)$ with $\phi_{\mathrm{s}2}$ are displayed in Figs. 8–10, respectively. As observed from Fig. 8*a*, the addition of $\phi_{\mathrm{s}2}$ increases the skin friction coefficient for $\epsilon < 0$, which contradicts the behaviour observed for $\epsilon > 0$. Meanwhile, the Nusselt number decreases as $\phi_{\mathrm{s}2}$ increases, as shown in Fig. 8*b*. The increase in $\phi_{\mathrm{s}2}$ is expected to boost the Nusselt number, which corresponds to the heat transfer rate, due to the increase in thermal conductivity. However, the results obtained may be due to the internal heat generation that increases the hybrid nanofluid temperature and decreases the temperature gradient at the surface; hence, the Nusselt number decreases.

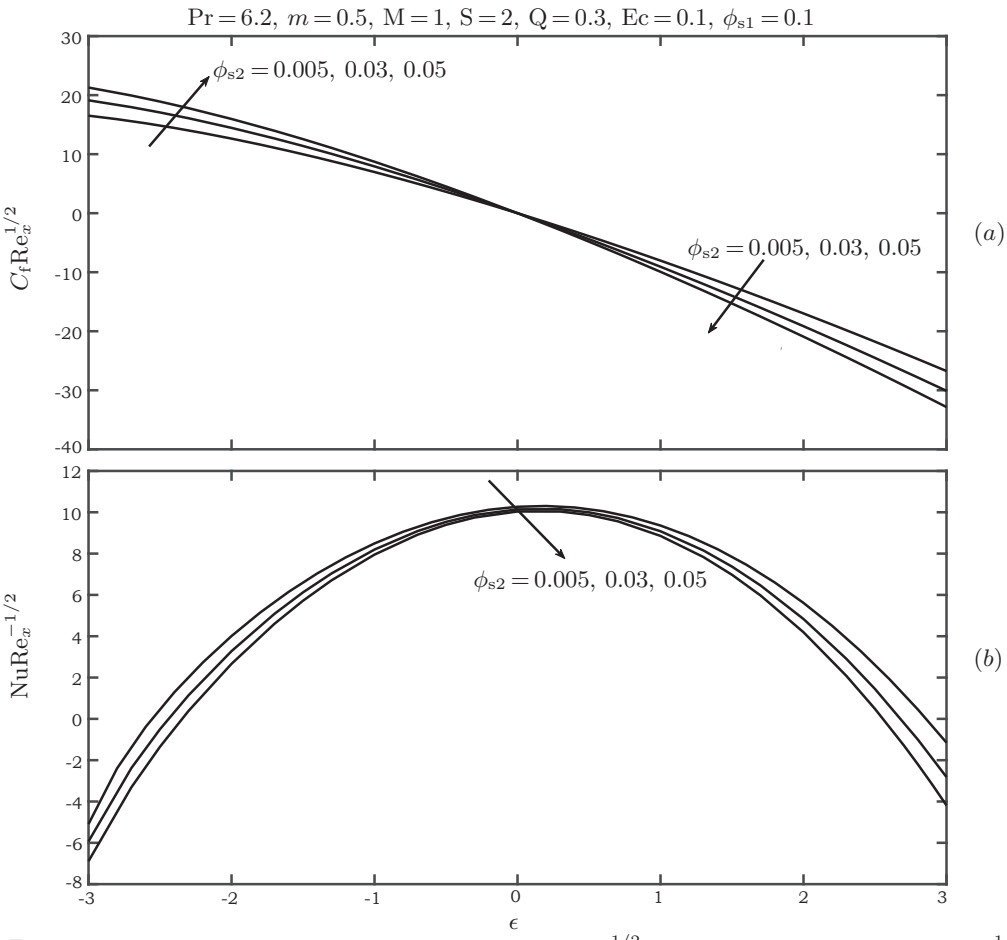

Fig. 8. Variation of (a) skin friction coefficient $C_{\mathrm{f}}\mathrm{Re}_x^{1/2}$ and (b) Nusselt number $\mathrm{NuRe}_x^{-1/2}$ with different values of ϕ_{s2}.

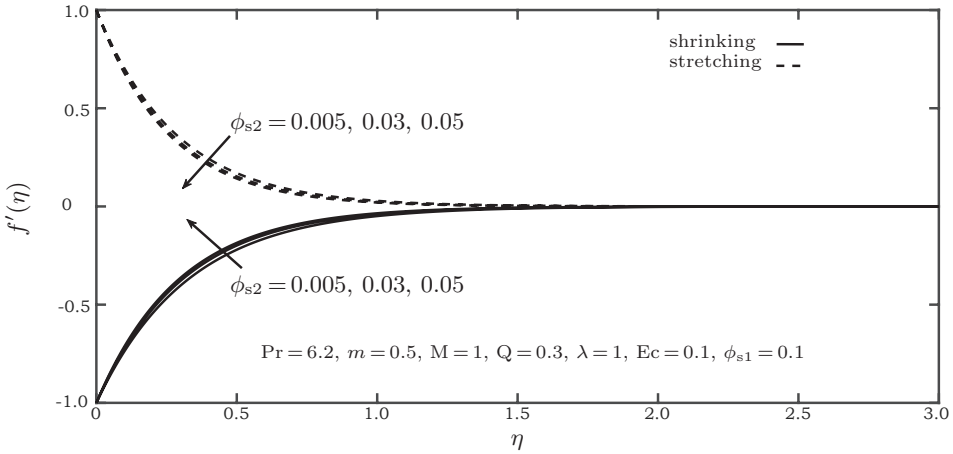

Fig. 9. Velocity profiles, $f'(\eta)$ with different values of ϕ_{s2}.

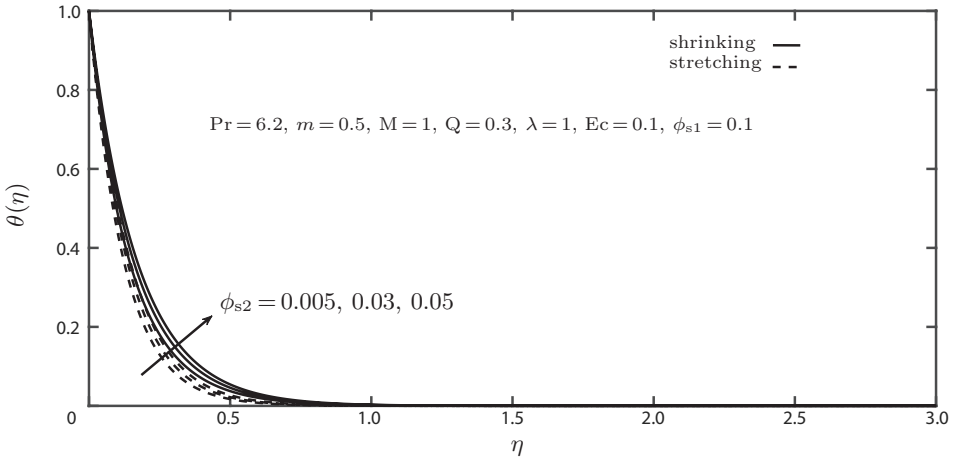

Fig. 10. Temperature profiles, $\theta(\eta)$ with different values of ϕ_{s2}.

The same behaviour is reported by Zainal *et al.* [20], where the heat generation is said to interrupt the interaction between the nanoparticles and decreases the thermal conductivities. In Fig. 9, the increase in ϕ_{s2} is noted to reduce the momentum boundary

Table 4. Values of $C_f \mathrm{Re}_x^{1/2}$ and $\mathrm{NuRe}_x^{-1/2}$ when $\mathrm{M} = 1, \mathrm{S} = 2, \mathrm{Ec} = 0.1, \mathrm{Pr} = 6.2$ and $m = 0.5$.

Working fluid	ϕ_{s1}	ϕ_{s2}	Q	λ	ϵ	$C_f \mathrm{Re}_x^{1/2}$	$\mathrm{NuRe}_x^{-1/2}$
Ag-CuO/H_2O	0.1	0.03	0.3	0.8	1.0	-8.832818	9.120770
				1.0	1.0	-9.076011	9.081970
					2.0	-19.145324	4.833540
					3.0	-30.098550	-2.816955
					-1.0	7.925850	8.195709
					-2.0	14.453729	3.278634
					-3.0	19.121557	-5.929110
				1.2	1.0	-9.309734	9.044598
			0.5	1.0		-9.076011	8.888198
			-0.3			-9.076011	9.626429
					2.0	-19.145324	5.525967
					-1.0	7.925850	8.882848
					-2.0	14.453729	4.551570
CuO/H_2O	0.1	0	0.3	1.0	1.0	-7.830843	9.411593
					-1.0	6.783636	8.550768
			-0.3		1.0	-7.830843	9.905811
					-1.0	6.783636	9.174516
Ag/H_2O	0	0.1	0.3	1.0	1.0	-9.532422	8.859699
					-1.0	8.421532	8.072282
			-0.3		1.0	-9.532422	9.371652
					-1.0	8.421532	8.703220
Pure water	0	0	0.3	1.0	1.0	-5.396631	9.963600
					-1.0	4.658501	9.225838
			-0.3		1.0	-5.396631	10.336475
					-1.0	4.658501	9.688772

layer thickness that causes the velocity profile to increase for the shrinking plate and to decrease for the stretching plate. Meanwhile, the values of $\theta(\eta)$ are augmented by the increase in ϕ_{s2}, as depicted in Fig. 10. According to [3], the nanoparticles dissipate energy in the form of heat. Thus, adding more nanoparticles will increase the heat energy that increases the hybrid nanofluid temperature and then thickens the thermal boundary layer. In Table 4, pure water has the lowest values of $|C_f \mathrm{Re}_x^{1/2}|$, followed by CuO/H_2O nanofluid, Ag-CuO/H_2O hybrid nanofluid, and Ag/H_2O nanofluid. These show that dispersing high thermal conductivity metallic Ag nanoparticles in a base fluid produces a nanofluid with a high skin friction coefficient, which requires high energy consumption (e.g., pumping power) in real life applications. Thus, hybridizing CuO nanoparticles into the Ag/H_2O nanofluid can assist in decreasing the skin friction coefficient for effective energy consumption. However, the current study shows that the Nusselt number is the highest for pure water, followed by CuO/H_2O nanofluid, Ag-CuO/H_2O hybrid nanofluid, and Ag/H_2O nanofluid. Again, these trends are due to the internal heat generation/absorption and viscous-Ohmic dissipation present in the flow problem.

The Eckert number

$$\mathrm{Ec} = \frac{u_w^2}{(C_p)_f (T_w - T_\infty)},$$

a dimensionless parameter used to characterize heat transfer dissipation, is defined as the ratio of kinetic energy to enthalpy difference of the boundary layer. Qasim and Noreen [36] stated that $\mathrm{Ec} = 0$ describes the absence of dissipation, the positive value of Ec describes the heat transfer from the plate to the fluid (plate cooling when $T_w > T_\infty$), and the negative value of Ec corresponds to the transfer of heat from the fluid to the plate (plate heating when $T_w < T_\infty$). It is observed from Fig. 11 that the increase in Ec decreases the rate of the heat transfer denoted by the Nusselt number. However, the temperature profile increases with Ec, as seen in Fig. 12. The increase in Ec enhances the conversion of kinetic energy into internal energy, increases the hybrid nanofluid temperature and thickens the thermal boundary layer. Since the increase in Ec decreases the temperature gradient at the surface, the heat transfer rate between the plate and the hybrid nanofluid becomes slower. Rapid cooling of the plate can be achieved by making the value of Ec as small as possible.

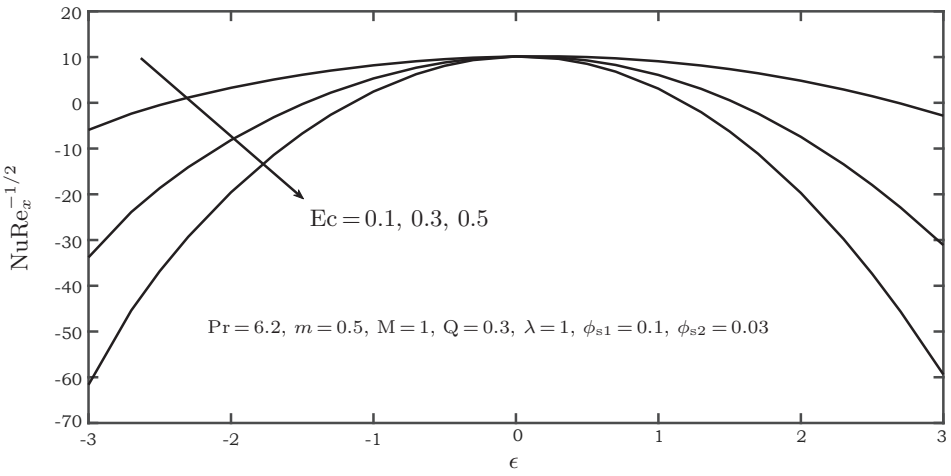

Fig. 11. Variation of $\mathrm{NuRe}_x^{-1/2}$ with different values of Ec.

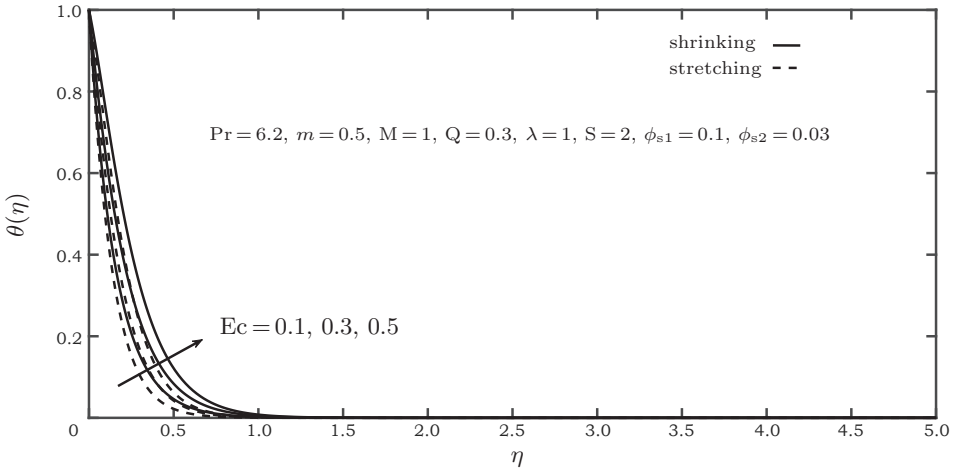

Fig. 12. Temperature profiles, $\theta(\eta)$ with different values of Ec.

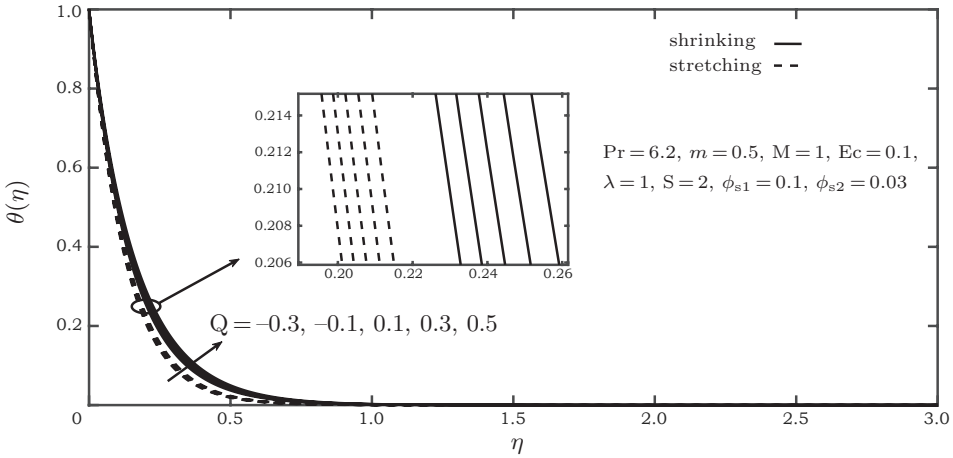

Fig. 13. Temperature profiles, $\theta(\eta)$ with different values of Q.

The values of $C_{\mathrm{f}}\mathrm{Re}_x^{1/2}$ and $\mathrm{Nu}\mathrm{Re}_x^{-1/2}$ with different values of the heat generation/absorption parameter Q are presented in Table 4. It is seen that the increase in Q does not have a significant impact on the skin friction coefficient, but the Nusselt number decreases as Q increases. The heat transfer rate is the highest in the presence of heat absorption ($\mathrm{Q} < 0$) and consequently decreases with heat generation ($\mathrm{Q} > 0$). The increase in the magnitude of the heat absorption parameter decreases the fluid temperature, whereas the increase in the heat generation parameter boosts the fluid temperature. Nanoparticles can increase the fluid temperature, and the presence of heat generation will further increase the hybrid nanofluid temperature, as observed in Fig. 13. With the existence of heat generation, extra heat is generated at the boundary layer, which increases the hybrid nanofluid temperature and enlarges the thermal boundary layer thickness; this decreases the temperature gradient at the surface and decreases the Nusselt number (see Table 4).

The impact of λ on the profiles of $f'(\eta)$ and $\theta(\eta)$ is then displayed in Figs. 14 and 15, respectively. The increase in the local porosity parameter λ increases the velocity

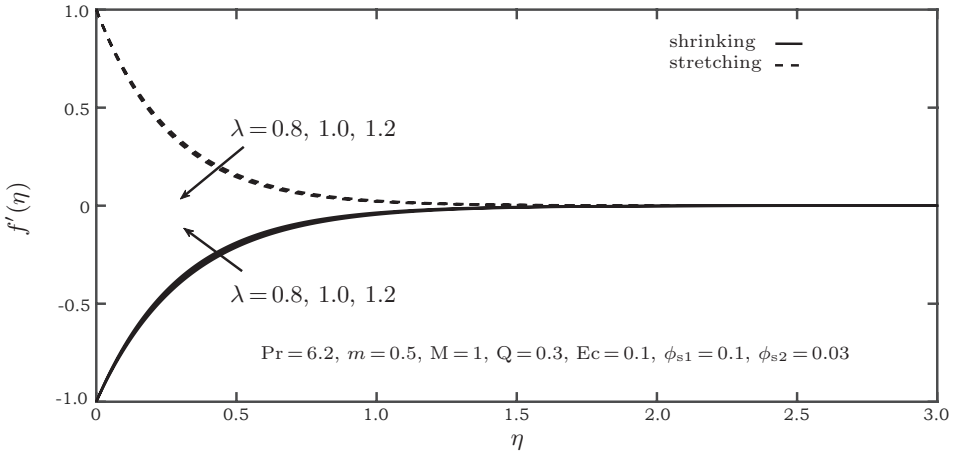

Fig. 14. Velocity profiles, $f'(\eta)$ with different values of λ.

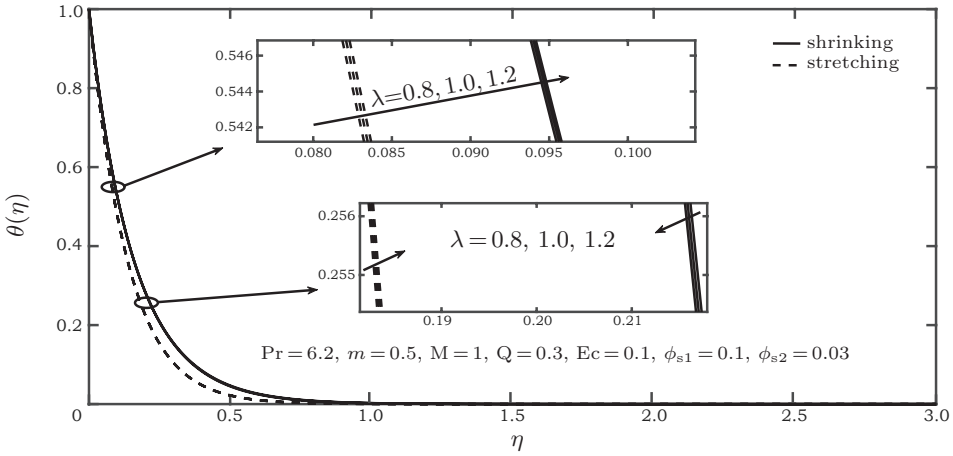

Fig. 15. Temperature profiles, $\theta(\eta)$ with different values of λ.

profile and reduces the momentum boundary layer thickness for the shrinking plate case, whereas in the stretching plate case, the velocity profile and the momentum boundary layer thickness reduce when λ increases. Moreover, for the stretching plate, the increase in λ decreases the velocity gradient at the surface and then decreases the value of $C_f \mathrm{Re}_x^{1/2}$, which is consistent with the results obtained in Table 4. Meanwhile, the hybrid nanofluid temperature shows an increase near the plate surface when λ increases. At some distance, the opposite behaviour is observed for the shrinking plate, where the fluid temperature decreases when λ increases; this is based on the temperature profile obtained in Fig. 15.

Finally, the variation of the velocity and temperature profiles with the stretching/shrinking parameter ϵ is depicted in Figs. 16 and 17, respectively. The increase in the stretching parameter ($\epsilon > 0$) enhances the magnitude of the skin friction coefficient, as shown in Table 4. Since the values of $C_f \mathrm{Re}_x^{1/2}$ are negative for the stretching plate, this implies that the stretching plate exerts a drag force on the hybrid nanofluid. In contrast, the drag force on the shrinking plate is exerted by the hybrid nanofluid, and the values of $C_f \mathrm{Re}_x^{1/2}$ get larger as the shrinking parameter ($\epsilon < 0$) increases. However, the increase in ϵ decreases the Nusselt number, and the Nusselt number for the stretching

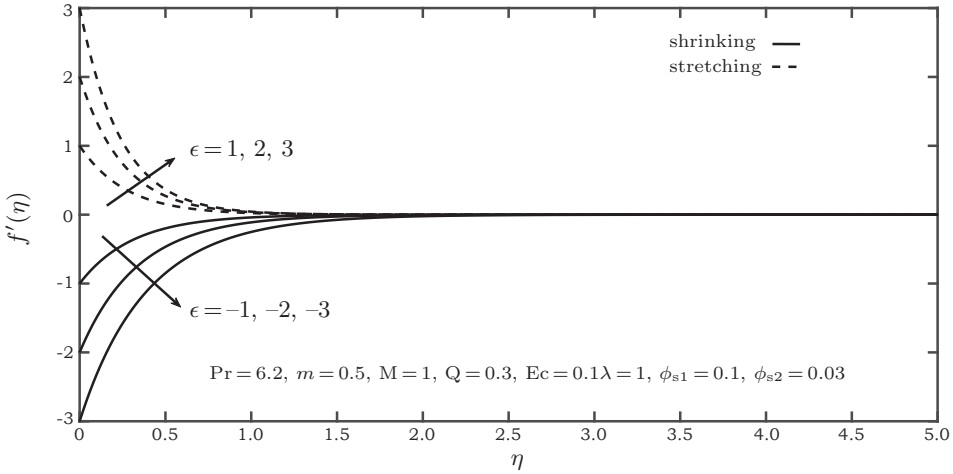

Fig. 16. Velocity profiles, $f'(\eta)$ with different values of ϵ.

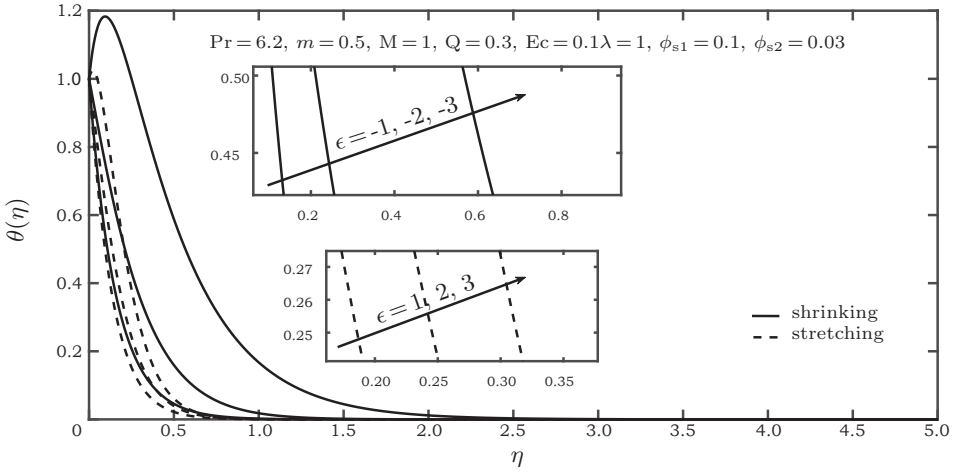

Fig. 17. Temperature profiles, $\theta(\eta)$ with different values of ϵ.

plate is higher than for the shrinking plate. Based on Fig. 16, the increase in ϵ is seen to enlarge the momentum boundary layer thickness that increases the velocity profile for the stretching plate and decreases the velocity profile for the shrinking plate. Nevertheless, the thermal boundary layer thickness and the temperature profile increase with ϵ. The increase in the stretching/shrinking parameter improves the momentum boundary layer thickness, which may enhance the effects of viscous-Ohmic dissipation in the flow that causes the hybrid nanofluid temperature to rise and, hence, to produce the profiles obtained in Fig. 17. The impact of ϵ on $\theta(\eta)$ is more significant in the shrinking plate case, which explains the smaller temperature gradient that results in a slower heat transfer rate at the surface and in a lower Nusselt number than in the stretching plate case.

Conclusions.

The MHD flow of an aqueous Ag-CuO hybrid nanofluid past a porous stretching/shrinking plate with suction is analyzed. The current flow problem considers the effects of heat generation/absorption and viscous-Ohmic dissipation. These parameters

are found to disturb the efficiency of the Ag-CuO/H_2O hybrid nanofluid, in such, the high thermal conductivity of the hybrid nanofluid does not affect the heat transfer rate. Meanwhile, the temperature of the hybrid nanofluid increases due to these parameters. Besides, the following behaviours are observed.

- The magnitude of the skin friction coefficient for the shrinking plate case is augmented by the increase in M, S and ϕ_{s2}, but the opposite situation occurred for the stretching plate case.
- The Nusselt number increases as S increases, but then it decreases when M, ϕ_{s2}, Ec, ϵ and λ increase.
- The Nusselt number for $Q < 0$ (heat absorption) is higher when compared to $Q > 0$ (heat generation).

In this flow problem, pure water was found to have the highest heat transfer rate compared to other nanofluids (Ag/H_2O and CuO/H_2O) and Ag-CuO/H_2O hybrid nanofluid. Therefore, pure water is the most efficient working fluid to be used as a coolant when heat generation and viscous-Ohmic dissipation are present in the flow. Further research can be carried out to find the ideal amount of Ag and CuO nanoparticles for the Ag-CuO/H_2O hybrid nanofluid to perform efficiently as the working fluid under the stated conditions.

Acknowledgements.
This work was supported by the Ministry of Higher Education Malaysia [KPT-FRGS/1/2019/STG06/UPM/02/3, Vot 5540309].

References

[1] J.A.R. Babu, K.K. Kumar and S.S. Rao. State-of-art review on hybrid nanofluids. *Renew. Sustain. Energy Rev.*, vol. 77 (2017), pp. 551–565.

[2] H. S Chahregh and S. Dinarvand. TiO2-Ag/blood hybrid nanofluid flow through an artery with applications of drug delivery and blood circulation in the respiratory system. *Int. J. Numer. Method H.*, (2020).

[3] V. Rajesh, A Chamkha and M. Kavitha. Numerical investigation of Ag-CuO/water hybrid nanofluid flow past a moving oscillating cylinder with heat transfer. *Math. Meth. Appl. Sci.*, (2020).

[4] I. Uddin, M.A. Khan, S. Ullah, S. Islam, M. Israr and F. Hussain. Characteristics of buoyancy force on stagnation point flow with magneto-nanoparticles and zero mass flux condition. *Results Phys.*, vol. 8 (2018), pp. 160–168.

[5] A.A.A. Arani and H. Aberoumand. Stagnation-point flow of Ag-CuO/water hybrid nanofluids over a permeable stretching/shrinking sheet with temporal stability analysis. *Powder Technol.*, vol. 380 (2021), pp. 152–163.

[6] W.N. Mutuku and O.D. Makinde. Double stratification effects on heat and mass transfer in unsteady MHD nanofluid flow over a flat surface. *Asia Pac. J. Comput. Engin.*, vol. 4 (2017), no. 1, pp. 1–16.

[7] S.P.A. Devi and S.S.U. Devi. Numerical investigation of hydromagnetic hybrid Cu–Al2O3/water nanofluid flow over a permeable stretching sheet with suction. *Int. J. Nonlin. Sci. Num.*, vol. 17 (2016), no. 5, pp. 249–257.

[8] S. Nadeem and N. Abbas. On both MHD and slip effect in micropolar hybrid nanofluid past a circular cylinder under stagnation point region. *Can. J. Phys.*, vol. 97 (2019), no. 4, pp. 392–399.

[9] E.H. Aly and I. Pop. MHD flow and heat transfer over a permeable stretching/shrinking sheet in a hybrid nanofluid with a convective boundary condition. *Int. J. Numer. Method H.*, (2019).

[10] I. Waini, A. Ishak and I. Pop. MHD flow and heat transfer of a hybrid nanofluid past a permeable stretching/shrinking wedge. *Appl. Math. Mech.*, vol. 41 (2020), no. 3, pp. 507–520.

[11] U. Yashkun, K. Zaimi, N.A.A. Bakar, A. Ishak and I. Pop. MHD hybrid nanofluid flow over a permeable stretching/shrinking sheet with thermal radiation effect. *Int. J. Numer. Method H.*, (2020).

[12] C. Jimenez, H. Vargas and R. Correa. Velocity profiles of ferrofluids in a cylindrical container and in the presence of external rotating magnetic fields of high strength and frequency. *Magnetohydrodynamics*, vol. 56 (2020), no. 4, pp. 341–368; DOI: http://doi.org/10.22364/mhd.56.4.1

[13] V. Klüber, L. Bühler and C. Mistrangelo. Numerical investigation of liquid metal flow in square channels under inclined magnetic fields for fusion relevant parameters. *Magnetohydrodynamics*, vol. 56 (2020), no. 2-3, pp. 149–156; DOI: http://doi.org/10.22364/mhd.56.2-3.6

[14] J. Mao, M. Jin and C. Xu. Numerical simulation of magnetohydrodynamic laminar flow in an electrically conducting circular pipe with V-shaped strips. *Magnetohydrodynamics*, vol. 57 (2021), no. 1, pp. 3–16; DOI: http://doi.org/10.22364/mhd.57.1.1

[15] K. Vajravelu and J. Nayfeh. Hydromagnetic convection at a cone and a wedge. *Int. Commun. Heat Mass Transf.*, vol. 19 (1992), no. 5, pp. 701–710.

[16] Z. Uddin, M. Kumar and S. Harmand. Influence of thermal radiation and heat generation/absorption on MHD heat transfer flow of a micropolar fluid past a wedge considering hall and ion slip currents. *Therm. Sci.*, vol. 18 (2014), no. suppl. 2, pp. 489–502.

[17] D. Pal. Magnetohydrodynamic viscous–Ohmic dissipation performance on unsteady convective heat transfer over a stretching surface in existence of internal heat generation/absorption. *Int. J. Comput. Meth. Eng. Sci. Mech.*, vol. 20 (2019), no. 4, pp. 308–318.

[18] T. Hayat and S. Nadeem. Heat transfer enhancement with Ag–CuO/water hybrid nanofluid. *Results Phys.*, vol. 7 (2017), pp. 2317–2324.

[19] T. Hayat, S. Nadeem and A.U. Khan. Numerical analysis of Ag–CuO/water rotating hybrid nanofluid with heat generation and absorption. *Can. J. Phys.*, vol. 97 (2019), no. 6, pp. 644–650.

[20] N.A. Zainal, R. Nazar, K. Naganthran and I. Pop. Heat generation/absorption effect on MHD flow of hybrid nanofluid over bidirectional exponential stretching/shrinking sheet. *Chin. J. Phys.*, vol. 69 (2021), pp. 118–133.

[21] T. Nabil and D.R. Mostapha. Hall current and joule heating effects on peristaltic flow of a Sisko fluid with mild stenosis through a porous medium in a tapered artery with slip and convective boundary conditions. *Sains Malays*, vol. 49 (2020), no. 5, pp. 1175–1190.

[22] J.W.S. Raj and S.P.A. Devi. Numerical analysis of nonlinear radiation, viscous and Ohmic dissipation effects on steady Magnetohydrodynamic forced convection flow over a shrinking surface with internal heat generation/absorption. *Int. J. Sci. Res. Math. Stat. Sci.*, vol. 7 (2020), pp. 9–16.

[23] R. Jusoh, K. Naganthran, A. Jamaludin, M.H. Ariff, M.F.M. Basir and I. Pop. Mathematical analysis of the flow and heat transfer of Ag-Cu hybrid nanofluid over a stretching/shrinking surface with convective boundary condition and viscous dissipation. *Data Analytics and Applied Mathematics (DAAM)*, vol. 1 (2020), no. 01, pp. 11–22.

[24] L.A. Lund, Z. Omar, I. Khan, A.H. Seikh, E.M. Sherif and K.S. Nisar. Stability analysis and multiple solution of Cu–Al2O3/H2O nanofluid contains hybrid nanomaterials over a shrinking surface in the presence of viscous dissipation. *J. Mater. Res. Technol.*, vol. 9 (2020), no. 1, pp. 421–432.

[25] N.S. Khashi'ie, N.M. Arifin, R. Nazar, E.H. Hafidzuddin, N. Wahi and I. Pop. Magnetohydrodynamics (MHD) axisymmetric flow and heat transfer of a hybrid nanofluid past a radially permeable stretching/shrinking sheet with Joule heating. *Chin. J. Phys.*, vol. 64 (2020), pp. 251–263.

[26] U. Yashkun, K. Zaimi, A. Ishak, I. Pop and R. Sidaoui. Hybrid nanofluid flow through an exponentially stretching/shrinking sheet with mixed convection and Joule heating. *Int. J. Numer. Method H.*, (2020).

[27] L. Yan, S. Dero, I. Khan, I. A. Mari, D. Baleanu, K.S. Nisar, E.M. Sherif and H.S. Abdo. Dual solutions and stability analysis of magnetized hybrid nanofluid with joule heating and multiple slip conditions. *Processes*, vol. 8 (2020), no. 3, p. 332.

[28] B. Mahanthesh, S.A. Shehzad, T. Ambreen and S.U. Khan. Significance of Joule heating and viscous heating on heat transport of MoS_2–Ag hybrid nanofluid past an isothermal wedge. *J. Therm. Anal. Calorim.*, vol. 143 (2021), no. 2.

[29] T. Hayat, S. Nawaz, A. Alsaedi and M. Rafiq. Mixed convective peristaltic flow of water based nanofluids with Joule heating and convective boundary conditions. *PLoS One*, vol. 11 (2016), no. 4, p. e0153537.

[30] L.F. Shampine, J. Kierzenka, M.W. Reichelt *et al.* . Solving boundary value problems for ordinary differential equations in MATLAB with `bvp4c`. *Tutorial Notes*, vol. 2000 (2000), pp. 1–27.

[31] M. Ferdows, G. Murtaza, J.C. Misra, E.E. Tzirtzilakis and A. Alsenafi. Dual solutions in biomagnetic fluid flow and heat transfer over a nonlinear stretching/shrinking sheet: Application of lie group transformation method. *Math. Biosci. Eng.*, vol. 17 (2020), no. 5, pp. 4852–4874.

[32] H. Upreti, A.K. Pandey and M. Kumar. MHD flow of Ag-water nanofluid over a flat porous plate with viscous-Ohmic dissipation, suction/injection and heat generation/absorption. *Alex. Eng. J.*, vol. 57 (2018), no. 3, pp. 1839–1847.

[33] E.M.A. Elbashbeshy, T.G. Emam, M.S. El-Azab, K.M. Abdelgaber. Laminar boundary layer flow along a stretching cylinder embedded in a porous medium. *Int. J. Phys. Sci.*, vol. 7 (2012), no. 24, pp. 3067–3072.

[34] N. Arifin, R. Nazar and I. Pop. Viscous flow due to a permeable stretching/shrinking sheet in a nanofluid. *Sains Malays.*, vol. 40 (2011), no. 12, pp. 1359–1367.

[35] P.S. Reddy and P. Sreedevi. Impact of chemical reaction and double stratification on heat and mass transfer characteristics of nanofluid flow over porous stretching sheet with thermal radiation. *Int. J. Ambient Energy*, (2020), pp. 1–11.

[36] M. Qasim and S. Noreen. Heat transfer in the boundary layer flow of a Casson fluid over a permeable shrinking sheet with viscous dissipation. *Eur. Phys. J. Plus*, vol. 129 (2014), no. 1, pp. 1–8.

Received 15.07.2021